NMPC-Based Orbit and Formation Control for an Earth-Gravity Monitoring Mission

72nd International Astronautical Congress (IAC), Dubai, United Arab Emirates, 25-29 October 2021.

IAC-21,D1,2,2,x64320

NMPC-Based Orbit and Formation Control for an Earth-Gravity Monitoring Mission

M. Boggio[a]*, P. Cotugno[a], C. Perez Montenegro[a], M. Pagone[a], C. Novara[a], L. Massotti[b]

[a] *Department of Electronics and Telecommunications, Politecnico di Torino, Corso Duca degli Abruzzi, 24, 10129, Torino, Italy*, mattia.boggio@polito.it, patrizia.cotugno@studenti.polito.it, carlos.perez@polito.it, michele.pagone@polito.it, carlo.novara@polito.it
[b] *ESA/ESTEC, Keplerlaan 1, 2201 AZ Noordwijk, The Netherland*, luca.massotti@esa.int
* Corresponding Author

Abstract

In the last decades, an increasing attention has been devoted to space gravimetric missions, with the goal of improving the understanding of Earth's mass change phenomena. One of the main objectives of these missions consists in measuring the temporal variations of the Earth gravity field over a long-time span, with very high spatial and temporal resolutions. In this context, the paper focuses on a gravity monitoring mission featuring a formation with two satellites following each other on the same orbit and each of them drag compensated. The aim is to design a formation control which is able both to counteract bias and drift of the residual drag-free accelerations and to reach the orbit and formation long-term stability. At this purpose, a Nonlinear Model Predictive Control (NMPC) framework is considered. A key element of this control technique is the use of an internal prediction model for finding an optimal trajectory over a finite time interval. Here, an Integrated Formation Control (IFC) model, based on a novel set of Hill-type equations, has been used. This model allows a common description of the formation altitude and inter-satellite distance, by defining a specific orbital reference frame called Formation Local Orbital Frame (FLOF). The ESA Next Generation Gravity Mission (NGGM), as part of the ESA-NASA cooperation in the frame of the MAGIC (Mass Change and Geosciences International Constellation), is considered as a benchmark for the developed NMPC framework. In this regard, a high-fidelity nonlinear model, with the 30th order gravity field and various atmospheric disturbances (e.g., atmospheric drag and solar pressure), has been used. Furthermore, to simulate a realistic situation, the issues related to the transmission of data between satellites is also considered by assuming long sampling times of the measurements due to absence of a radio-frequency inter-satellite link. Such lack of data has been dealt with the implementation of orbit propagators, which are able to propagate, on board of each satellite, position and velocity of the companion spacecraft. The novelty of these propagators is the ability to compute accurately the companion satellite orbit, despite being designed considering a low order gravity field and completely neglecting other atmospheric disturbances. The obtained results demonstrate the effectiveness of the proposed NMPC strategy and show its capability to guarantee long-term stability, despite the lack of companion satellite information and a low command effort.

Keywords: NMPC, Autonomous Guidance, Control, NGGM, Orbit Propagator, Formation

Nomenclature

M: Total Torque
I_m: Inertia Matrix
q: Body Attitude Quaternion
a_{CoM}: Center of Mass Acceleration
ΔV: Delta-V
μ: Earth's planetary constant
g_0: Earth's gravity acceleration at sea level
I_{sp}: Specific impulse
J: Generic cost function
L: True longitude
m: Mass
r: Orbit radius
p: Semilatus rectum
T: Thrust
T_p: Prediction horizon
T_s: Sampling time
u: Acceleration
v: Velocity
f_{drag}: Drag Force
f_{sun}: Solar Pressure
u_{form}: Formation Control
g: Gravity Acceleration (30th Order Term of Spherical Harmonics)
g_4: Gravity Acceleration (4th Order Term of Spherical Harmonics)

Acronyms/Abbreviations

NMPC: Nonlinear Model Predictive Control
IFC: Integrated Formation Control
FLOF: Formation Local Orbital Frame
NGGM: Next Generation Gravity Mission
LAGEOS: Laser Geodynamics Satellite
GRACE: Gravity Recovery and Climate Experiment
GOCE: Gravity Field and steady-state Ocean Circulation Explorer

EMC: Embedded Model Control
ESA: European Space Agency
RF ISL: Radio-Frequency Inter-Satellite Link
CoM: Center of Mass
LEO: Low Earth Orbit
CoP: Center of Pressure
NGA: National Geospatial-Intelligence Agency
GNSS: Global Navigation Satellite System
MPC: Model Predictive Control
RHC: Receding Horizon Control
SSL: Satellite-to-Satellite Line
LTI: Linear Time-Invariant
SQP: Sequential Quadratic Programming

1. Introduction

In the first decades of the XXI century an increasing attention has been devoted to space gravimetric missions. The main purpose of this type of missions consists in measuring with high accuracy and resolution the value of the Earth's gravity field while monitoring its changes in time and space. As a matter of fact, the Earth's gravitational field is not constant and homogeneous over the entire surface of our planet, but it specifically depends on the mass distribution among all its layers. As a result, the measure of the gravity field could be an important instrument of information about the morphology and the density of all the different parts of the Earth, from its interiors to the crust, also involving the atmosphere [1]. Since the value of this measure is influenced by mass change phenomena, it results evident the reason that pushes the research to place ever greater emphasis on this type of studies. Indeed, mass changes phenomena are strictly linked with all the climate variables, and their observation and monitoring enable the investigation on all those geophysical processes which involve hydrology (total water storage and cycles), tectonic plates displacement, changes in the mass of ice sheets, ocean and atmosphere circulation, and so forth.

In order to observe mass distribution changes and transport in and between the different Earth's system layers (Atmosphere, Oceans, Hydrosphere, Cryosphere, and Solid Earth), the most direct way consists in measuring the temporal variations of the Earth gravity field over a long-time span [2]. Since gravity constraints the motion of Earth's satellites, studying the perturbations introduced in their orbits can give us a good source of information to measure the gravitational field [3]. At this purpose, in the last 50 years different satellites dedicated to geodesy have been conceived. The first that fits inside this context is the LAGEOS (Laser Geodynamics Satellite), launched in 1976 [4]. It made use of very low altitude satellites and novel measurement techniques to provide a measure of the gravity field with good spatial and temporal resolution. Nevertheless, it is especially in the last 20 years that many steps forward have been made in this direction thanks to the progresses given by the successful US-German gravity missions GRACE (Gravity Recovery and Climate Experiment, launched in 2002 [5]), GRACE Follow-On [6] and the European GOCE (Gravity Field and steady-state Ocean Circulation Explorer, launched in 2009 [7], [8]) mission.

In order to increase at a higher degree the recovery of the gravity field, future Earth gravimetry missions will fact as free falling proof masses and will measure the inter-satellite distance variations via a laser interferometer instrument [9], for revealing anomalies and variations of the local gravity field. This ambitious goal can be reached considering long-distance distributed space systems, in the order between 100 and 220 km distance (as in GRACE FO), but possibly at lower altitude (down till 350 km). Given that at those altitudes the effects of the residual Earth atmosphere are very severe, this kind of missions require "drag-free" satellites and an accurate distance measurement system [1], [10].

In this context, the paper focuses on an Earth-gravity monitoring mission featuring a formation with two drag-free satellites. In order to make the spacecraft only affected by local gravity, that is to counteract the atmospheric drag, pre-designed linear and angular drag-free controllers are employed. They are based on the Embedded Model Control (EMC) [11], [12], an efficient and robust technique for model-based design capable of stabilizing systems affected by parametric and structural uncertainties. However, given the impossibility of a perfect drag-free condition, due to some secular (low frequency) residual accelerations, a formation control is needed. In this regard, the aim of our work is to design a formation control which is able both to counteract bias and drift of the residual drag-free accelerations and to reach the orbit and formation long-term stability. The approach adopted in the formation control design is based on the Nonlinear Model Predictive Control (NMPC) [13] methodology. The idea comes from the need of developing an optimal control law managing, at the same time, state and input constraints due to the numerous formation scientific requirements and the limited thruster range. Indeed, besides the formation requirements, also the very low thruster authority and the need to cancel the drag-free residual acceleration strongly constraint the problem under study. A key element of the NMPC is an internal prediction model, used to find an optimal trajectory over a finite time interval. Here, an integrated formation control (IFC) model, based on a novel set of Hill-type equations, has been developed and used. This model allows a common description of the formation altitude and inter-satellite distance, by defining a specific orbital reference frame called Formation Local Orbital Frame (FLOF).

The Next Generation Gravity Mission (NGGM) pair is considered as a benchmark for the developed NMPC framework. The concept of NGGM has been proposed by ESA with the aim to improve the work started by the

previous gravimetric missions, like GOCE and GRACE. Indeed, relying on the heritage gained from these two successful missions, NGGM sets its goal in the measurement of the variations of the Earth's gravity field, over a long-time span, with spatial and temporal resolution [14]. In this regard, to emulate the NGGM mission, a high-fidelity nonlinear model, with the 30th order gravity field and various atmospheric disturbances (e.g., atmospheric drag and solar pressure), has been used for the long-run simulations.

Furthermore, to consider an even more realistic situation, the issues related to the transmission of data between satellites is also taken into account by assuming long sampling times of the measurements due to absence of a radio-frequency inter-satellite link (RF ISL). As a result, the position and velocity information of the companion spacecraft is propagated on board of each satellite in the time intervals during which no real-time information is available (e.g., 1 orbit). To deal with such lack of data, orbit propagators with low computational complexity are implemented. The novelty of these propagators is the ability to compute accurately the companion satellite orbit, despite being designed considering a low order gravity field (J4) and completely neglecting other atmospheric disturbances.

The paper is organized as follows. In Section 2, an overview about the nonlinear model developed in Simulink for the NGGM mission is presented. In Section 3, the design of the orbit and formation control by means of NMPC methodology is described. Section 4 deals with the introduction of the innovative low-fidelity orbit propagators. The simulations results are presented in Section 5. At last, the conclusions are drawn in Section 6.

2. NGGM Model

The NGGM will consist in a formation of a pair of satellites, placed in a near-polar orbit at an altitude between 350 and 500 km. The nonlinear model used for simulation purposes has been developed in Simulink and is composed of three main blocks: one block for each satellite and the third one used to generate the nominal variables of FLOF. As shown in Figure 1, the model of each satellite includes three parts: a first block is devoted for simulating the satellite kinematics and dynamics and for deriving the orbital elements; a second block is used to model the atmospheric and gravity disturbances (forces and torques) acting on the satellite, and a last block is used to model the measurement instruments and metrology systems adopted by each spacecraft for measuring and monitoring the variables of interest.

Going more into detail, the satellite kinematics and dynamics have been modelled treating the satellites as rigid bodies which move with respect to some inertial frame. In the simulator, the attitude dynamics block implements the Euler moment equation, which, starting from total torque $\boldsymbol{M}$ acting on the spacecraft and given the inertia matrix I_m, returns the simulated angular velocity and acceleration of the spacecraft in the body frame:

$$I_m \dot{\boldsymbol{\omega}} = \boldsymbol{M} - \boldsymbol{\omega} \times I_m \boldsymbol{\omega} \tag{1}$$

The angular velocity exiting from the attitude dynamics block becomes the input of the attitude kinematic block, which, according to the following equation, gives as output the body attitude quaternion

$$\dot{q} = \frac{1}{2} q \otimes \boldsymbol{\omega}^q \tag{2}$$

where $\boldsymbol{\omega}^q = (0, \boldsymbol{\omega})$ is the quaternion translation of the angular velocity $\boldsymbol{\omega}$.

The non-gravitational body forces, as well as gravity forces, are used by the Orbit Dynamics block to compute the satellite CoM acceleration $\boldsymbol{a}_{CoM}$ and, by integration, the satellite CoM velocity and position. These quantities, together with the angular momentum, are finally needed to obtain the six classical orbital elements ($a, e, i, \Omega, arg, \theta$), through which it is possible to completely describe the orbit of a satellite and its position on it.

The block used to model the atmospheric and gravity disturbances takes as input the simulated satellite position and velocity coming from the dynamics and kinematics block. Among all the environmental forces and torques acting on the satellite, the disturbances that significantly affect the spacecraft are the Aerodynamic Drag and the Solar Pressure, described in the following.
The Atmospheric Drag can be seen as the friction which opposes the spacecraft velocity vector. Since it is proportional to the density, which decreases exponentially with the altitude, it represents a significant disturbance especially in Low Earth Orbits (LEO). In this study, to model this disturbance force, each spacecraft has been considered made by a number of flat surfaces, result of a trade-off between the computational load and the smoothness of forces and torques profiles. Each surface is identified by its normal unit vector and its centre. The contribution given by each tile to the total drag force depends on the element surface, the relative wind velocity, and the air density. For these reasons, the Drag Model block takes as input the body wind velocity and the body angular rate and computes the relative velocity of each flat surface. Then, the contributions of each surface are combined in order to obtain the overall drag force and torque. For the computation of the aerodynamic coefficient, two models can be adopted to describe the kind of interaction between the body and the air flow taking into account, eventually, the momentum transfer between the gas particle and the surface element:

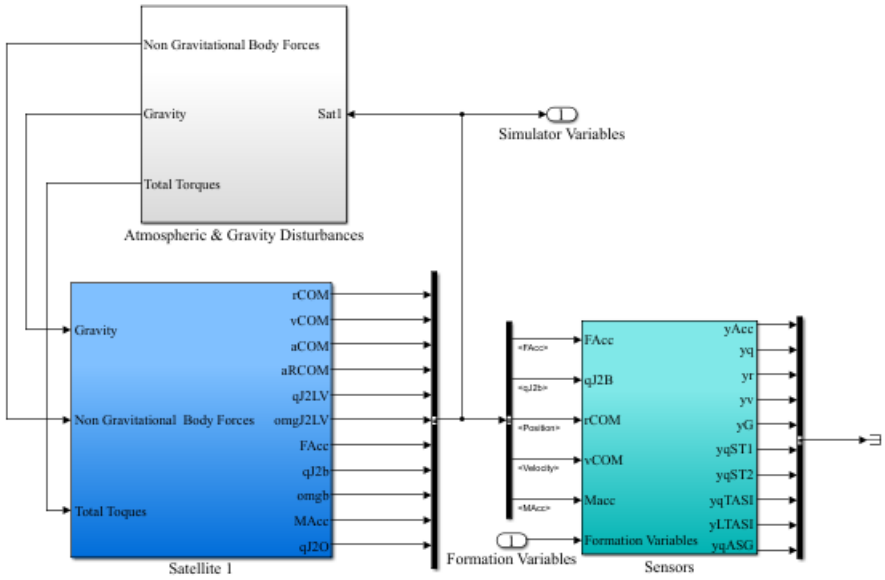

Fig. 1. Nonlinear Model of a Single Satellite

1. The Hyper-thermal model, in which the particles move in straight lines parallel to the airflow and only those surfaces directly invested by the airflow contribute to the definition of the aerodynamic coefficients.
2. The Thermal model, in which the particles motion is not parallel to the airflow direction and also the shadowed surfaces contribute to the definition of the aerodynamic coefficients.

In the present study the thermal model has been adopted as it considered the best fitting of the drag experienced in flight by GOCE [15]. Note that, even if the drag force is a distributed load, it can be considered as an equivalent concentrated force applied in a point called Centre of Pressure (CoP). Therefore, the drag force produces also a torque having magnitude proportional to the lever arm, that is the distance between CoM and CoP.

As previously said, the second important atmospheric disturbance considered here is the solar radiation pressure, that is the mechanical pressure exerted upon the spacecraft surfaces due to the exchange of momentum between the spacecraft and the electromagnetic field. The inputs of the model used to compute this disturbance force are the spacecraft position and the sun position. In particular, the latter is needed to take into account that only those surfaces that are directly exposed to the sun give a not null contribution. Consequently, a coefficient that varies between 0 and 1 has been introduced in order to consider the degree of exposure of each surface to the solar radiations. For each tile, the solar pressure force $\boldsymbol{F}_{rk}$ is computed by combining specular reflections, diffuse reflections, and total absorption. Finally, as done for the atmospheric disturbance, the overall sun force and torque are obtained by summing the contributions of all the spacecraft surfaces.

Besides the atmospheric disturbances, the forces and torques acting on the spacecrafts also include the gravity. Indeed, the Earth gravity field interacts with the satellite generating a force that, applied in the CoM, determines the body orbit, and a torque that acts as an attitude perturbation. In the nonlinear model presented here, the gravity model is obtained considering the spherical harmonic representation of planetary gravity at a specific location. The planetary model that has been adopted is EGM2008, that is the latest Earth spherical harmonic gravitational model from National Geospatial-Intelligence Agency (NGA). The spherical harmonic representation is needed to consider a more accurate model of the Earth gravitational field than the one that can be obtained by considering a spherical gravity model, which ideally assumes the Earth mass concentrated in its centre as in a central force field. Since the measure of the Earth gravitational field is the target of NGGM, for this study a spherical harmonic expansion of high degree ($k = 30$) has been used in order to guarantee an accurate description of its influence.

As previously said, a second contribution given by the Earth gravity field is the gravity gradient torque. This torque is due to the nonuniform gravity forces acting on extended bodies and can be expressed as

$$\overrightarrow{M_g} = \int_B \vec{s} \times \vec{g}(\vec{r}) dm \tag{3}$$

where B is the body volume, and $\vec{s}$ the difference between the mass position $\vec{r}$ and the spacecraft CoM position.

Finally, we can briefly summarize the measurement instruments and metrology systems involved in the monitoring of the variables of interest. They may roughly be subdivided into three main categories:

- Inertial navigation sensors, such as accelerometers and gyroscopes, that are mostly used to detect acceleration and angular rate variations.
- Position and navigation sensors, such as the Global Navigation Satellite System [GNSS], needed to measure the spacecraft position and velocity by observing the motion of the spacecraft CoM with respect to the GNSS constellation.
- Attitude sensors, such as Sun and Earth sensors, star trackers and magnetometers, that are used to measure the satellite attitude.

All the mentioned sensors have been modelled by summing a noise to the clean signal. For instance, the accelerometer model is composed by a filtered high frequency noise to which bias and drift have been added.

3. Formation Control

This paper is focused on the development of a NMPC framework for the formation control of a gravimetric mission. As previously said, the Next Generation Gravity Mission has been considered as a benchmark for this purpose. In particular, the inline formation type, in which the two satellites fly on same nominal orbit with different true anomalies, has been taken into account. The ambitious goal of the formation control consists in guaranteeing the long-term stability of the system by simultaneously counteracting bias and drift of residual drag-free accelerations. Indeed, due to some secular residual accelerations, a perfect drag-free condition cannot be achieved. As described by the requirements collected in Table 1, the control strategy shall allow the concurrent monitoring of both satellites' altitude and relative distance in order to ensure that perturbations affecting these two quantities remain bounded during the entire mission lifetime, namely a solar cycle. These requirements, splitted into distance, radial and lateral variations, are expressed in terms of percentage with respect to the nominal altitude and distance values.

To face the problem, a NMPC-based framework has been implemented. The Model Predictive Control (MPC), also called Receding Horizon Control (RHC) is a modern feedback strategy widely adopted for industry applications, especially for linear processes. This control technique can find an optimal control law managing at the same time state and input constraints and providing an online adaptation of the control strategy to possible variations of the process conditions. However, since many systems are, in general, inherently nonlinear, linear models are often inadequate to represent the behaviour of the system. This is the rationale behind the NMPC, which is a variant of the standard MPC based on nonlinear models and/or nonlinear constraints.

Table 1. NGGM Formation Control Requirements

Variable	Bound	Unit
Formation distance variation	$\eta_d = 10\%$	% (distance)
Formation radial variation	$\eta_r = 2\%$	% (altitude)
Formation lateral variation	$\eta_y = 1\%$	% (distance)

In detail, consider the following nonlinear system:

$$\begin{aligned} \dot{x}(t) &= f(x(t), u(t)) \\ y(t) &= h\big(x(t), u(t)\big), \end{aligned} \tag{4}$$

where $x \in \mathbb{R}^{n_x}$, $u \in \mathbb{R}^{n_u}$, $y \in \mathbb{R}^{n_y}$ are the state, the input and the output, respectively. We assume that the state is measured, with a sampling time T_s. If this assumption does not hold, an observer can be employed. The measurements are $x(t_k)$, $t_k = T_s k$, $k = 0, 1, \dots$. At each time $t = t_k$, a prediction of the system state and output over the time interval $[t, t + T_p]$ is performed, where $T_p > T_s$ is the prediction horizon. The prediction is obtained by integrating the equation (4). At any time $\tau \in [t, t + T_p]$, the predicted output $\hat{y}(\tau) \equiv \hat{y}\big(\tau, x(t), u(t{:}\,\tau)\big)$ is a function of the 'initial' state $x(t)$ and the input signal. The notation $u(t{:}\,\tau)$ is used to indicate the input signal in the interval $[t, \tau]$. At each time $t = t_k$, we look for an input signal $u^*(t{:}\,\tau)$, minimizing a suitable cost function $J\left(u\big(t{:}\,t + T_p\big)\right)$ subject to possible constraint that may occur during the system's operations. Mathematically, at each time $t = t_k$, the following optimization problem is solved:

$$\begin{aligned} & u^*\big(t{:}\,t + T_p\big) = \underset{u(\cdot)}{arg\,min}\, J\left(u\big(t{:}\,t + T_p\big)\right) \\ & subject\ to{:} \\ & \dot{\hat{x}}(\tau) = f\big(\hat{x}(\tau), u(\tau)\big), \quad \hat{x}(t) = x(t) \\ & \hat{y}(\tau) = h\big(\hat{x}(\tau), u(\tau)\big) \\ & \hat{x}(\tau) \in X_C, \ \ \hat{y}(\tau) \in Y_C, \ \ u(\tau) \in U_C \end{aligned} \tag{5}$$

where X_C, Y_C, and U_C are suitable sets describing possible constraints on the state, output, and input respectively. The performance index J is a weighted quadratic function of the predicted output tracking error $\tilde{y}_P$ and the system input u:

$$J\left(u(t:t+T_p)\right) = \int_t^{t+T_p} \|\tilde{y}_P(\tau)\|_Q^2 + \|u(\tau)\|_R^2 \, d\tau + \left\|\tilde{y}_P(t+T_p)\right\|_P^2. \quad (6)$$

The $\|v\|_W^2$ notation represents the (square) weighted norm of a vector $v \in \mathbb{R}^n$ such that $\|v\|_W^2 \doteq v^T \boldsymbol{W} v = \sum_{i=i}^n w_i v_i^2$ and $\boldsymbol{W} = \text{diag}(w_1, \dots, w_n) \in \mathbb{R}^n$, $w_i \geq 0$. The predicted tracking error is $\tilde{y}_P(\tau) = r(\tau) - \hat{y}(\tau)$, whereas $r(\tau)$ is the desired reference to track and $\hat{y}(\tau)$ is obtained by integration of equation (4). The weights $\boldsymbol{Q} \geq 0, \boldsymbol{P} \geq 0$, and $\boldsymbol{R} > 0$ are diagonal matrix. Note that $\boldsymbol{Q}, \boldsymbol{P} \in \mathbb{R}^{n_y \times n_y}$ and $\boldsymbol{R} \in \mathbb{R}^{n_x \times n_x}$. A receding control horizon strategy is employed: at a given time $t = t_k$, only the first optimal input is applied to the plant, while the remainder of the solution is discarded. Then, the complete procedure is repeated at the next time $t = t_{k+1}$.

Remark. The optimization problem in equation (5) is in general numerically not tractable, since $u(\cdot)$ is a continuous-time signal and thus the number of decision variables is infinite. To overcome this issue, a finite parametrization of the input signal $u(\cdot)$ has been employed. In particular, we assumed a piece-wise constant parametrization, with changes of values at the nodes $\tau_1, \dots, \tau_{n_N} \in [t, t+T_p]$. Several simulations have been carried out, considering values of n_N from 1 to 6. It has been observed that the value $n_N = 1$ leads to satisfactory behavior, without any significant performance degradation but with a reduced computational complexity with respect to the case $n_N > 1$. Hence, this value (corresponding to a constant input for every $\tau \in [t, t+t_p]$) has been assumed for all simulation of Section 5.

The Model Predictive Control, being a particular branch of model-based design, is based on the idea to employ a dynamical model of the plant to predict the future behaviour of the variables of interest and compute an optimal control command. In this paper, for the NMPC internal prediction an integrated formation control (IFC) model, based on a novel set of Hill-type equations, has been developed and used. This model allows a common description of the formation altitude and inter-satellite distance, and is based on the so-called triangular virtual structure, depicted in Figure 2, and on the definition of a specific orbital reference frame called Formation Local Orbital Frame (FLOF).

The FLOF is built from the GNSS range measurements, and its axes are defined as follows:

$$\boldsymbol{o}_1 = \frac{\Delta \boldsymbol{r}}{d}, \quad \boldsymbol{o}_2 = \frac{\frac{\boldsymbol{r}}{r} \times \boldsymbol{o}_1}{\left|\frac{\boldsymbol{r}}{r} \times \boldsymbol{o}_1\right|}, \quad \boldsymbol{o}_3 = \boldsymbol{o}_1 \times \boldsymbol{o}_2 \quad (7)$$

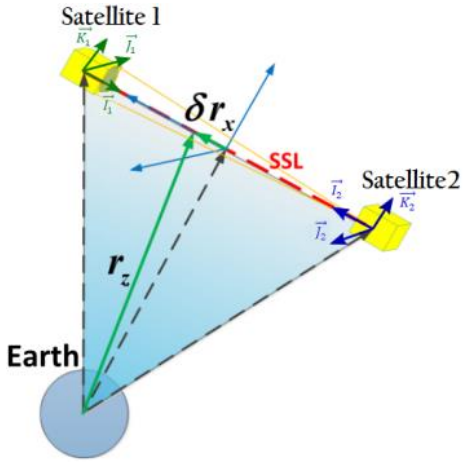

Fig. 2. NGGM Triangular Structure and Formation Local Orbital Frame

where $\boldsymbol{r} = (\boldsymbol{r}_1 + \boldsymbol{r}_2)/2$ is the main formation radius, $\Delta \boldsymbol{r} = (\boldsymbol{r}_1 - \boldsymbol{r}_2)$ is the satellite relative position and $d = |\Delta \boldsymbol{r}|$ is the inter-satellite distance.

The model formulation assumes that the high-frequency acceleration components are only due to the gravity term. This assumption holds if the short-term non gravitational accelerations are cancelled by means of a drag-free control. Looking at Figure 2, the satellite-to-satellite distance variations are measured along the satellite-to-satellite line (SSL), which is defined as the line connecting the CoM of the satellites, assuming the presence of a proper attitude and pointing control system able to keep aligned the two satellites optical axis.

To build the integrated formation model, a preliminary definition of formation and orbit perturbations is needed. At this purpose, let's introduce, in the formulation of the formation mean and differential radius, the three Cartesian perturbations $\delta d, \delta r_x, \delta r_z$:

$$\begin{aligned} \Delta \boldsymbol{r} &= (d_{nom} + \delta d)\overrightarrow{o_1} \\ \boldsymbol{r} &= r_x \overrightarrow{o_1} + r_z \overrightarrow{o_3} = (0 + \delta r_x)\overrightarrow{o_1} + (r_{nom} + \delta r_z)\overrightarrow{o_3} \end{aligned} \quad (8)$$

where d_{nom} is the nominal inter-satellite distance and r_{nom} stands for the nominal formation altitude. Moreover, besides $\delta d, \delta r_x, \delta r_z$, let's define three other perturbations provided by the 3D non-zero components of the FLOF angular rate vector $\boldsymbol{\omega} = \omega_x \overrightarrow{o_1} + \omega_y \overrightarrow{o_2} + \omega_z \overrightarrow{o_3}$, whose norm is defined as $\omega = \omega_{nom} + \delta\omega$. As it is evident by the presence of 6 perturbations, the overall formation dynamics will be described by 6 DoFs, and consequently the IFC model will involve six differential equations. The first set of differential equations is obtained starting from the relative position vector $\Delta \boldsymbol{r}$, while the second set of differential equations comes from the kinematic equation of the mean formation radius $\boldsymbol{r}$. The final perturbation equations have been obtained by combining the kinematics equations involving the six

selected perturbations with the formation triangle dynamic equations. It is worth to underline that, for simplicity, in the derivation of the IFC model, the gravity gradient $\Delta \boldsymbol{g}$ and the gravity term $\boldsymbol{g}$ have been expressed in FLOF coordinates considering only the spherical gravity term, ideally arranging the higher order terms, from J2 on, as part of the external acceleration contribution.

The obtained perturbation equations have been linearised around an equilibrium point, whose components are defined in the following:

$$\begin{aligned} d_{eq} &= d_{nom} \\ r_{z_{eq}} &= r_{nom} \\ r_{x_{eq}} &= 0 \\ \omega_{y_{eq}} &= \omega_{nom} \\ \omega_{x_{eq}} &= \omega_{z_{eq}} = 0 \end{aligned} \tag{9}$$

The obtained linearized equations can be expressed through the perturbed state variables and inputs, leading to the following linear time-invariant (LTI) continuous-time system:

$$\begin{aligned} \begin{bmatrix} \delta\dot{\boldsymbol{x}}_f \\ \delta\dot{\boldsymbol{v}}_f \end{bmatrix}(t) &= \omega_{nom} \begin{bmatrix} 0 & A_{12} \\ A_{21} & A_{22} \end{bmatrix} \begin{bmatrix} \delta\boldsymbol{x}_f \\ \delta\mathbf{v}_f \end{bmatrix}(t) \\ &+ \frac{1}{\omega_{nom}} \begin{bmatrix} 0 \\ B_2 \end{bmatrix} \boldsymbol{a}_f(t) \\ \mathbf{y}_f(t) &= [C_1 \; C_2] \begin{bmatrix} \delta\boldsymbol{x}_f \\ \delta\mathbf{v}_f \end{bmatrix}(t) \end{aligned} \tag{10}$$

where A_{12}, A_{21}, A_{22} and B_2 are parameter free matrices. The formation triangle perturbed state vector can be defined as the difference between the actual and the nominal values and it is composed by two sub-vectors: $\delta\boldsymbol{x_f}$ and $\delta\boldsymbol{v_f}$ that respectively represent the length and the rate state variables. Defining $\alpha = d_{nom}/r_{nom}$, the state vector and the non-gravitational acceleration input vector are given by:

$$\delta\boldsymbol{x}_f = \begin{bmatrix} \delta d = d - d_{nom} \\ \rho_x = \alpha r_x \\ \rho_z = \alpha(r_z - r_{nom}) \end{bmatrix},$$

$$\delta\boldsymbol{x}_f = \begin{bmatrix} \dfrac{\delta\dot{d}}{\omega_{nom}} \\ \dfrac{\dot{\rho}_x}{\omega_{nom}} \\ \dfrac{\delta\dot{\rho}_z}{\omega_{nom}} \\ w_x = \dfrac{\alpha\dot{r}_x}{\omega_{nom}} \\ w_y = \dfrac{d_{nom}(\omega_y - \omega_{nom})}{\omega_{nom}} \\ w_z = \dfrac{\alpha\dot{r}_z}{\omega_{nom}} \end{bmatrix}, \tag{11}$$

$$\boldsymbol{a}_f = \begin{bmatrix} \Delta a_x \\ \Delta a_y \\ \Delta a_z \\ \alpha a_x \\ \alpha a_y \\ \alpha a_z \end{bmatrix}$$

where α is used to express all the quantities in length unit and $a_x, a_y, a_z, \Delta a_x, \Delta a_y, \Delta a_z$ are the components of mean and differential accelerations

$$\boldsymbol{a} = \frac{\boldsymbol{a}_1 + \boldsymbol{a}_2}{2}, \qquad \Delta\boldsymbol{a} = \boldsymbol{a}_1 - \boldsymbol{a}_2 \,. \tag{12}$$

Now, from the complete model, it is possible to consider a restricted seventh order one, which is proven to be observable and controllable assuming $\mathbf{y}_f(t) = \delta\boldsymbol{x}_f(t)$. The state vector of the restricted model takes into account only the three Cartesian perturbations (ρ_x, ρ_z, δd) and their normalized rates ($w_x, w_z, w_d = \dot{d}/\omega_{nom}$), plus the normalized perturbation of the orbital rate w_y. In addition, also the input is restricted to the in-plane input variables. The obtained 7-th order LTI system is

$$\begin{aligned} \begin{bmatrix} \dot{\boldsymbol{r}} \\ \dot{\boldsymbol{w}} \end{bmatrix}(t) &= \begin{bmatrix} 0 & I\omega_{nom} \\ A_{21} & A_{22} \end{bmatrix} \begin{bmatrix} \boldsymbol{r} \\ \boldsymbol{w} \end{bmatrix}(t) + \begin{bmatrix} 0 \\ B_2 \end{bmatrix} \boldsymbol{u}(t) \\ \boldsymbol{y}(t) &= [I \;\; 0] \begin{bmatrix} \boldsymbol{r} \\ \boldsymbol{w} \end{bmatrix}(t), \qquad \begin{bmatrix} \boldsymbol{r} \\ \boldsymbol{w} \end{bmatrix}(0) = \begin{bmatrix} \boldsymbol{r}_0 \\ \boldsymbol{w}_0 \end{bmatrix} \end{aligned} \tag{13}$$

where

$$[\boldsymbol{r}\ \boldsymbol{w}]^T = \left[\rho_x, \rho_z, \delta d, w_x, w_z, w_d, w_y\right]^T,$$
$$\boldsymbol{u} = \left[u_{fx,} u_{fz}, \Delta u_{fx}, \Delta u_{fz}\right]^T = [\alpha a_x, \alpha a_z, \Delta a_x, \Delta a_z]^T,$$
$$A_{12} = 3\omega_{nom}\begin{bmatrix}1&0&0\\0&1&0\\0&1&0\\-1&0&0\end{bmatrix}, A_{22} = 2\omega_{nom}\begin{bmatrix}0&-1&1&0\\1&0&0&1\\0&0&0&1\\0&0&-1&0\end{bmatrix}, \quad (14)$$
$$B_2 = \begin{bmatrix}\alpha&0&0&1\\0&\alpha&0&0\\0&0&1&0\\0&0&0&-1\end{bmatrix}\Big/\omega_{nom}.$$

The NMPC controller has been implemented as a Simulink block able to perform the control algorithm previously described. For the internal prediction, the linearized model explained so far has been used. Looking at the IFC input vector $\boldsymbol{u}$, that is the NMPC control command, it is possible to note that in order to sum the formation control command with the other non-gravitational contributions (namely atmospheric disturbances and drag-free control commands), it is necessary to derive from the command input $\boldsymbol{u}$, the accelerations $\boldsymbol{a}_1$ and $\boldsymbol{a}_2$ given by the formation control to the single satellites:

$$\boldsymbol{a}_1 = \begin{bmatrix}a_{1x}\\a_{1y}\\a_{1z}\end{bmatrix} = \begin{bmatrix}\frac{2u_{fx}+\alpha\Delta u_{fx}}{2\alpha}\\0\\\frac{2u_{fz}+\alpha\Delta u_{fz}}{2\alpha}\end{bmatrix},$$
$$\boldsymbol{a}_2 = \begin{bmatrix}a_{2x}\\a_{2y}\\a_{2z}\end{bmatrix} = \begin{bmatrix}\frac{2u_{fx}-\alpha\Delta u_{fx}}{2\alpha}\\0\\\frac{2u_{fz}-\alpha\Delta u_{fz}}{2\alpha}\end{bmatrix}. \quad (15)$$

where the out-of-plane coordinates are obviously equal to zero.

For the choice of the best NMPC configuration, the relevant parameters to be tuned are the sampling time T_S, the prediction horizon T_P, the weight matrices Q, P and R, and the command lower and upper bounds L_b and U_b. At this purpose, the following guidelines have been taken into account:

- A sampling time T_s as large as possible needs to be considered in order to avoid interference with the wide-band drag-free control.
- The prediction horizon T_p can be obtained with a trial-and-error procedure, considering that generally a large T_p increases the closed-loop stability properties but a "too large" T_p may reduce the short time tracking accuracy.
- The command input must remain very limited in order to guarantee a very low thruster authority, consequently very stringent input constraints have to be used.
- A state constraint has to be included in the optimization problem in order to meet the requirement on the formation distance, as specified in Table 1.

For the solution of the optimization problem required by the NMPC technique, the Sequential Quadratic Programming (SQP) solver provided by the Matlab Nonlinear Optimization Toolbox® has been used.

4. Orbit Propagators

This section is aimed at introducing the main modelling concepts regarding the development of low-fidelity orbit propagators to be included in the nonlinear model previously described. The reason behind the realization of these orbit propagators regards the issues related to the transmission of measurement data between one satellite and its companion, due to the absence of a radio-frequency inter-satellite link (RF ISL) and the long sampling times of measurements (at least one orbit). This means that the information about position and velocity of, for example, Satellite 2 provided by GPS measurements becomes available on Satellite 1 once every orbital period. During the time intervals in which no real-time information is available, position and velocity of Satellite 2 need to be computed by means of the orbit propagator. Consequently, the Satellite 2 orbit propagator is embedded inside the Satellite 1 block scheme, as shown in Figure 3. The outputs of the orbit propagator are the propagated Satellite 2 velocity and position which will be used to derive the Formation Variables on board of Satellite 1. In the same way, on Satellite 2 will be present the orbit propagator of Satellite 1, whose outputs will be used to derive the Formation Variables on board of Satellite 2.

The novelty of these propagators is the ability to accomplish their task despite having been designed with a very low computational complexity. Indeed, to develop a very simple model, only the perturbations due to the gravity term have been taken into account, while completely neglecting all the other atmospheric disturbances.

In order to develop propagators capable of generating velocity and position as similar as possible to real ones, with the aim to compute the spacecraft orbit without impinging the capability of the control system to stabilize the formation virtual structure, it is necessary to obtain:

$$\boldsymbol{a}_{CoMp_i} \cong \boldsymbol{a}_{CoM_i} \quad (16)$$

where $i = 1,2$ denotes one of the two satellites, $\boldsymbol{a}_{CoMp_i}$ is the propagated acceleration of satellite i, while $\boldsymbol{a}_{CoM_i}$ is the real acceleration of satellite i. The real satellite acceleration $\boldsymbol{a}_{CoM}$ is given by the sum of the negative gravity acceleration $\boldsymbol{g}$ and all the non-gravitational accelerations which include the atmospheric disturbances

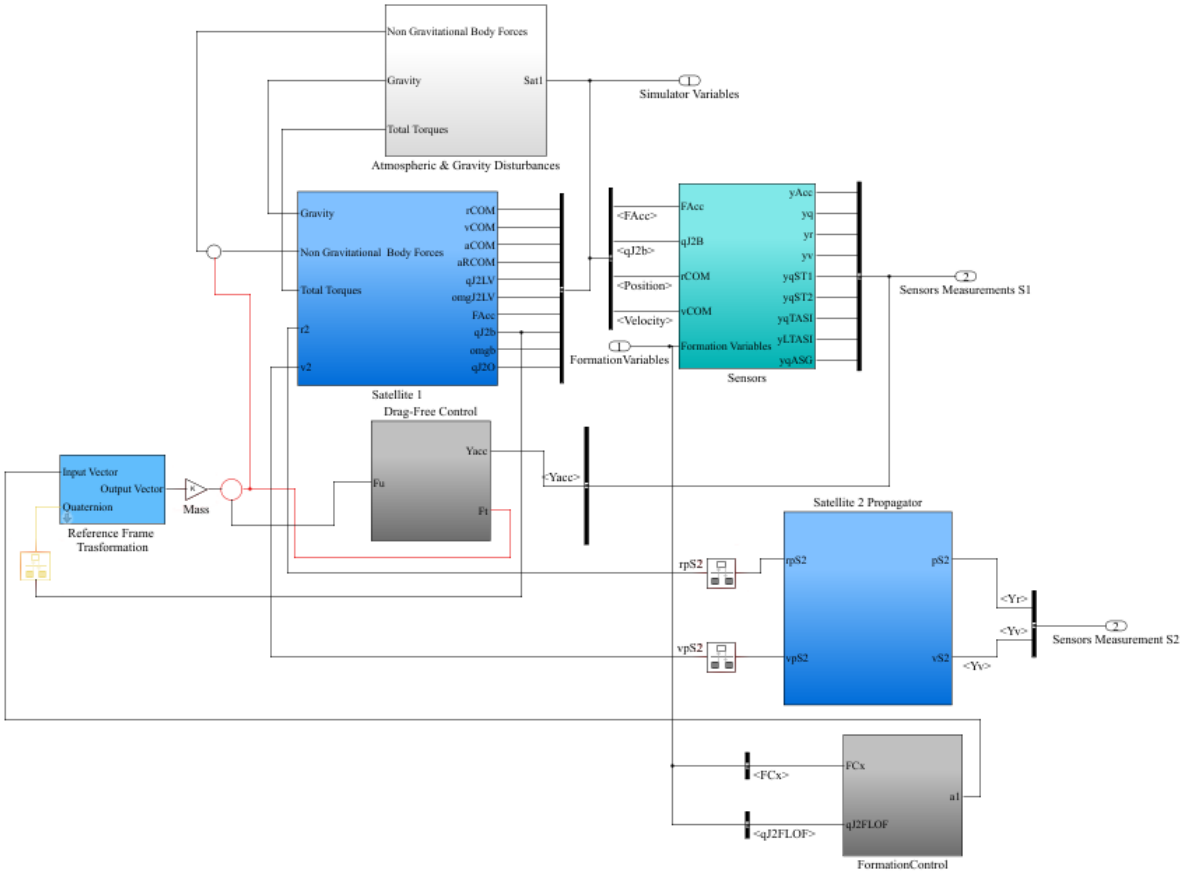

Fig. 3. Satellite 1 Block Scheme with Orbit Propagator

(e.g., drag force $\boldsymbol{f}_{drag}$ and solar pressure $\boldsymbol{f}_{sun}$) and the command actions of the drag-free control and the formation control $\boldsymbol{u}_{form}$:

$$\boldsymbol{a}_{CoM} = -\boldsymbol{g} + \frac{\boldsymbol{f}_{drag}}{m} + \frac{\boldsymbol{f}_{sun}}{m} + \frac{\boldsymbol{u}_{drag}}{m} + \frac{\boldsymbol{u}_{form}}{m} \quad (17)$$

Assuming that the drag-free control system is able to fulfil its task, that is the non-gravitational accelerations due to the atmospheric disturbances are zeroed by the drag-free command action, thus Eq. 17 becomes:

$$\boldsymbol{a}_{CoM} \cong -\boldsymbol{g} + \frac{\boldsymbol{u}_{form}}{m} \quad (18)$$

The approach adopted for the modelling of the orbit propagators presented in the following consists in a cascade of two integrators through which to derive the satellites propagated velocity and position starting from an approximated value of their acceleration. In particular, only the negative gravity term has been taken into account. Furthermore, it is worth noticing that the gravity model used inside the propagator is slightly different from the one adopted to simulate the real satellite orbital dynamics. Indeed, in the satellite nonlinear model the 30th order of spherical harmonics was used for the gravity force, while inside the orbit propagator a 4th order zonal coefficient has been adopted.

In our work, three type of orbit propagators have been developed:

1. Basic Orbit Propagator
2. Orbit Propagator with Command Action
3. Orbit Propagator with Error Correction

In the first configuration, shown in Figure 4a, only the gravity term has been considered. Then, the approximated value of satellite acceleration is:

$$\boldsymbol{a}_{CoMp_i} \cong -\boldsymbol{g}_{4i} \quad (19)$$

where i denotes one of the two satellites and $\boldsymbol{g}_4$ is used to indicate the gravity acceleration derived by means of the 4th order term of spherical harmonics. Note that, as shown in Figure 4, the two integrators used to propagate the satellite velocity and position are driven by means of a pulse generator whose frequency is the one to which the measurement data of the companion satellite become available on board of each spacecraft. This frequency is

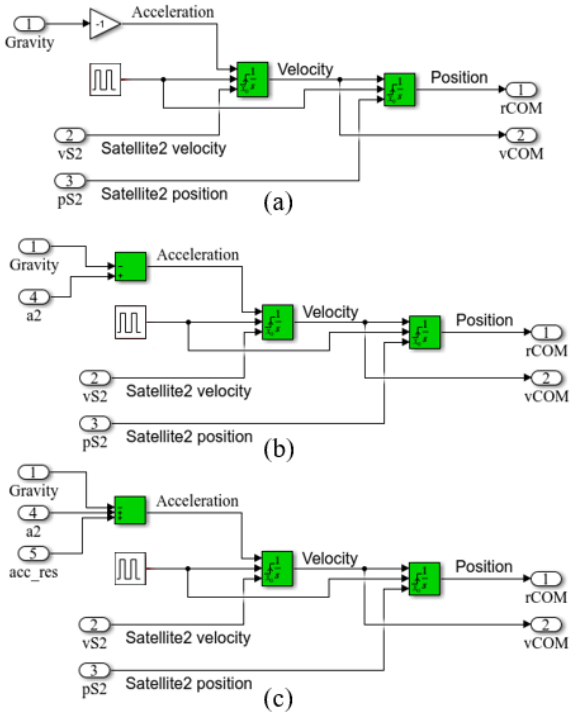

Fig. 4. a) Basic Orbit Propagator b) Orbit Propagator with Command Action c) Orbit Propagator with Error Correction

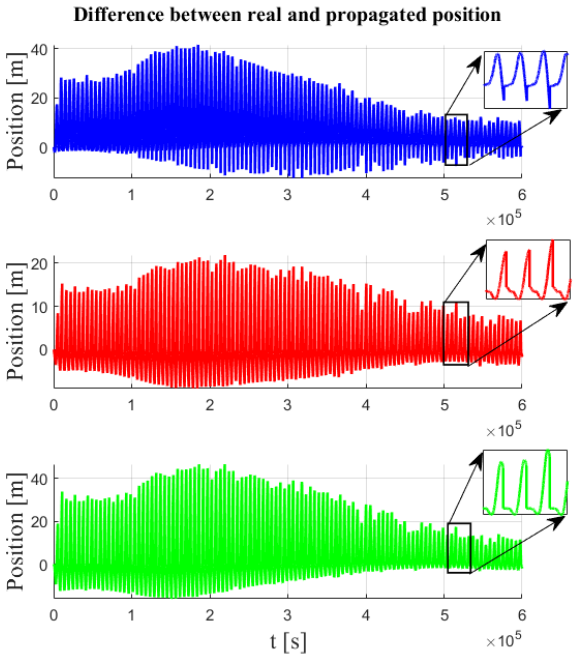

Fig. 5. Difference between real and propagated position of Satellite 2 – 1st, 2nd and 3rd components

also used to decide when the integrators initial conditions need to be updated during the simulation.

To reduce the difference between real and propagated accelerations, a first refinement consists of introducing, as input of the orbit propagator, the command acceleration coming from the formation control, as depicted in Figure 4b. In this way, the approximated value of satellite acceleration $\boldsymbol{a}_{CoMp}$ becomes:

$$\boldsymbol{a}_{CoMp_i} \cong -\boldsymbol{g}_{4i} + \frac{\boldsymbol{u}_{form_i}}{m} \tag{20}$$

As we can notice, this expression is very similar to the one in equation (17) with the only difference that the gravity term is obtained through a 4th order expansion of spherical harmonics.

To compensate this difference between gravity terms, it was decided to implement one last modification in the model just described. The idea is to include, on board of each spacecraft, two orbit propagators: one to compute the orbit of the companion spacecraft and the other one to provide the propagated acceleration of the spacecraft on which the orbit propagator is mounted. In this way, it is possible to exploit the error $\boldsymbol{a}_{res}$ between the real and propagated accelerations of one satellite to correct, at the next time instant, the orbit propagation of the other satellite. Then, this residual acceleration is defined as:

$$\begin{aligned} \boldsymbol{a}_{res} &= \boldsymbol{a}_{CoM} - \boldsymbol{a}_{CoM_p} \\ &= -\boldsymbol{g} + \frac{\boldsymbol{f}_{drag}}{m} + \frac{\boldsymbol{f}_{sun}}{m} + \frac{\boldsymbol{u}_{drag}}{m} + \frac{\boldsymbol{u}_{form}}{m} + \boldsymbol{g}_4 - \frac{\boldsymbol{u}_{form}}{m} \\ &\cong - -\boldsymbol{g} + \boldsymbol{g}_4 \end{aligned} \tag{21}$$

As can be seen, $\boldsymbol{a}_{res}$ provides the difference between the gravities computed using different orders expansion of spherical harmonics.

As illustrated in Figure 4c, after this last refinement, the final expression of the new propagated acceleration is:

$$\boldsymbol{a}_{CoMp_i} \cong \boldsymbol{a}_{res_j} - \boldsymbol{g}_{4i} + \frac{\boldsymbol{u}_{form_i}}{m} \tag{22}$$

where $i = 1,2$ denotes the propagated satellite and $j = 1,2$ (with $j \neq i$) indicates its companion.

In Figures 5-6 the differences, obtained considering the third type of propagator, between real and propagated velocity and position of Satellite 2 are reported, with the intent to draw attention on the effectiveness of the proposed model in the computation of the satellite orbit. As shown in figures, according to the modelling design, the three components of each quantity reset to zero as soon as a new measurement data becomes available (in this case a sampling time of one orbit is considered). The

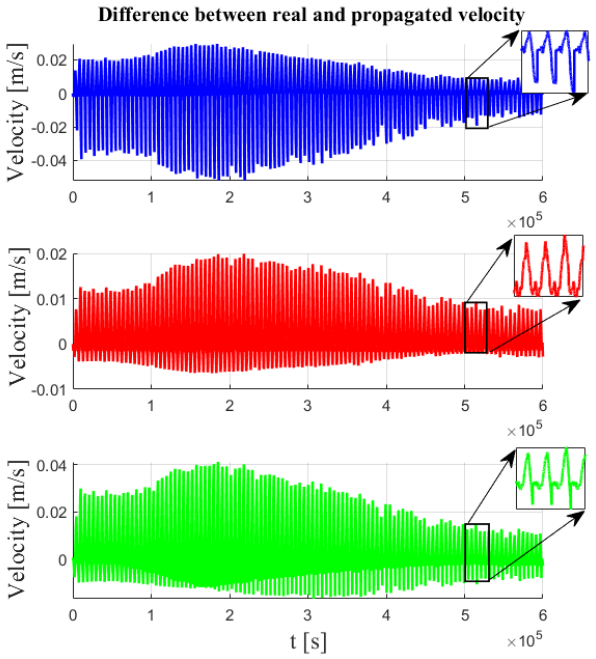

Fig.6. Difference between real and propagated velocity of Satellite 2 – 1st, 2nd and 3rd components

obtained results prove that the orbit propagators are able to provide a very good estimation of the satellite position maintaining the error in the range of few meters. Moreover, it is also possible to notice that in the long run this error begins to progressively decrease. For the sake of brevity, Figures 5-6 are referred only to Satellite 2, but obviously the same considerations hold also for Satellite 1.

5. Results

This section as the purpose to collect and present the simulated results obtained from a wide long-run simulation campaign performed before and after having introduced the orbit propagators above described. The results, presented here, have been obtained with the NMPC configuration reported in Table 2. The parameters in the table have been chosen with a trial-and-error procedure, considering the guidelines previously defined. In all the simulated conditions, the NGGM mission requirements, introduced in Table 1, have been checked. All the tests have been performed with a simulation time lasting for 2000 orbits.

According to the previous considerations, the prediction horizon has been chosen as close as possible to the orbital period, that is $T_P = 4000\ s$. This value turned out to be the best trade-off between closed-loop stability properties and tracking accuracy. Then, noting a certain linear dependence between the drag-free residual acceleration and the command input, stringent input constraints have been chosen in order to ensure a very

Table 2. NMPC configuration parameters and input constraints

Parameter	NMPC Configuration
T_s	$10\ s$
T_p	$4000\ s$
Q	$diag([1,1,1])$
P	$diag([1,1,1])$
R	$diag([0.5,0.5,0.5])$
L_b	$[-\alpha e^{-5}, -\alpha e^{-5}, -5e^{-5}, -5e^{-5}]$
U_b	$[\alpha e^{-5}, \alpha e^{-5}, 5e^{-5}, 5e^{-5}]$
Gravity	Order 30

small command effort, implying however a reduction of the sampling time up to $T_P = 10\ s$. Finally, the diagonal elements of the weight matrices have been selected in order to obtain a suitable trade-off between convergence time (P and Q matrices) and fuel consumption (R matrix).

By means of simulations the fulfilment of the mission requirements specified in Table 1 has been checked. In particular, the main objective has been to ensure the long-term stability of the lateral, radial and distance perturbations $(\delta r_x, \delta r_z, \delta d)$ though admitting 'natural' fluctuations around the altitude and distance nominal values.

In Figure 7, the bounds imposed on each variable by the formation requirements have been highlighted with a green line. The plot clearly shows that the three states do not diverge but remain inside the specified limits, thus it

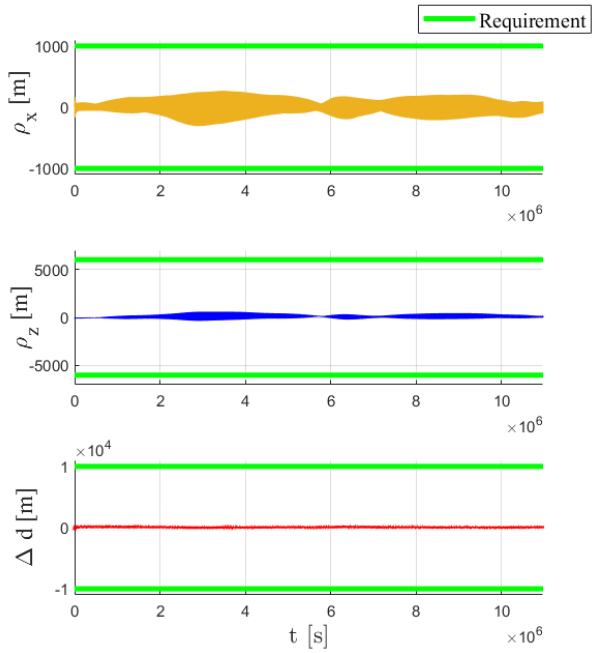

Fig. 7. Formation Radial, Lateral and Distance Variations

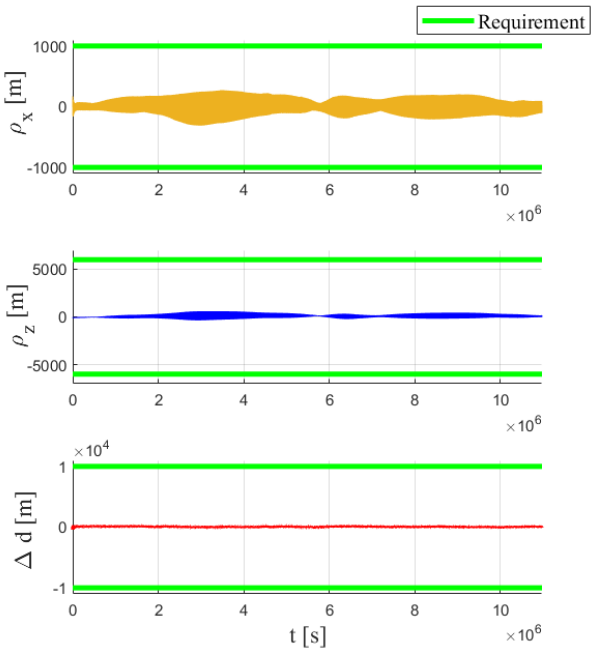

Fig. 8. Formation Radial, Lateral and Distance Variations with propagators

is possible to state that the developed NMPC framework is able to stabilize the system. In particular, the perturbation on the formation distance δd is close to zero and widely remains inside the specified bounds thanks to the control action and the state constraints introduced in the NMPC framework.

The same check has been performed after having included the orbit propagators, specifically the "Orbit Propagator with Error Correction" configuration, inside the nonlinear model. As we can notice from Figure 8, the simulated results are almost identical to those of Figure 7, proving the ability of the developed NMPC framework to stabilize the system and fulfill the requirements despite the lack of data due to the long sampling time of measurements. Simulations with orbit propagators have been performed considering a sampling time of measurements progressively increasing: 1 orbit, 3 orbits and 5 orbits. Beyond this value, the simulations began to show a performance degradation.

6. Conclusions

In summary, we have presented an alternative orbit and formation control for a new type of gravimetric missions, like NGGM under study by ESA. In particular, the paper focuses on two drag-free satellites flying in loose formation on a low-Earth orbit with the aim to measure temporal variations of the Earth gravity field over a long-time span. The design of the orbit and formation control is based on the NMPC. This control methodology allows to meet the requirements, managing at the same time state and input constraints. As internal prediction model, the Integrated Formation Control model, which exploits the concept of formation triangle and the Formation Local Orbital Frame, has been used. To simulate a realistic situation, the Next Generation Gravity Mission is considered as a benchmark for the developed NMPC framework. In this regard, a high-fidelity nonlinear model and the absence of a radio-frequency inter-satellite link have been taken into account. Besides, for overcoming the lack of data, orbit propagators with low computational complexity are implemented. The results, obtained after a long-run simulation campaign, prove the effectiveness of the proposed NMPC and show its capability to guarantee long-term stability, although the use of a very approximated internal model, lack of information about the companion satellite and low command effort.

Acknowledgements

The NMPC framework and its performance presented in this paper have been produced as a consultancy to the work package carried out by Thales Alenia Space under ESA contract of the study "NGGM Proof-of-Concept Test Results, Instrument and System – Requirements Extension of Work CCN2"

References

[1] S., Cesare, A., Allasio, A., Anselmi, S., Dionisio, S., Mottini, M., Parisch, L., Massotti, P., Silvestrin. "The European way to gravimetry: From GOCE to NGGM". Advances in Space Research 57.4 (Feb. 2016), pp. 1047–1064.

[2] R., Haagmans, C., Siemes, L., Massotti, O., Carraz, P., Silvestrin. "ESA's next-generation gravity mission concepts". Rendiconti Lincei. Scienze Fisiche e Naturali 31 (Jan. 2020).

[3] Y., Kozai. "The earth gravitational potential derived from satellite motion". Space Sci. Rev. 5 (1966), 818–879.

[4] B.D., Tapley, B.E., Schutz, R.J., Eanes. "Station coordinates, baselines, and earth rotation from LAGEOS laser ranging: 1976– 1984". J. Geophys. Res. 90 (1985), 9235–9248.

[5] M.R., Drinkwater, R., Floberghagen, R., Haagmans, D., Muzi, A., Popescu. "GOCE: ESA's first Earth Explorer Core mission". In the Space Science Series of ISSI (2003), vol. 18. Kluwer Academic Publishers.

[6] B.S., Sheard, G., Heinzel, K., Danzmann, D.A., Shaddock, W.M., Klipstein, W.M., Folkner. "Inter-satellite laser ranging instrument for the GRACE follow-on mission". J. Geod. 2021, 86, 1083-1095.

[7] B.D., Tapley, S., Bettadpur, J.C., Ries, P.F., Thompson, M.M., Watkins. "GRACE measurements of mass variability in the earth system". Science 305 (2004), 503–506.

[8] R., Floberghagen, M., Fehringer, D., Lamarre, D., Muzi, B., Frommknecht, C., Steiger, J., Piñeiro, A., da Costa. “Mission design, operation and exploitation of the gravity field and steady-state ocean circulation explorer mission”. J. Geodesy 2011, 85, 749-758.
[9] K., Nicklaus, S., Cesare, C., Dahl, L., Massotti, L., Bonino, S., Mottini, M., Pisani, P., Silvestrin. “Laser metrology concept consolidation for NGGM”. CEAS Space J. 2020.
[10] L., Massotti, G.B., Amata, A., Anselmi, S., Cesare, P., Martimort, P., Silvestrin. “Next generation gravity mission: Status of the design and discussion on alternative drag compensation scenarios. Proc. SPIE Remote Sens., Vol. 11530, 2020.
[11] E., Canuto. “Embedded Model Control: Outline of the theory”. ISA Transactions 46.3 (2007). pp. 363-377.
[12] L., Colangelo, L., Massotti, E., Canuto, C., Novara. “Embedded model control GNC for the Next Generation Gravity Mission”. Acta Astronautica (2017), vol. 140, pp. 497-508.
[13] R., Findeisen, F., Allgöwer. “An introduction to Nonlinear Model Predictive Control”. 2002.
[14] R., Koop, R., Rummel. “The Future of Satellite Gravimetry, Final Report of the Future Gravity Mission”. Workshop, 12–13 April 2007. ESA/ESTEC, Noordwijk, The Netherlands.
[15] S., Dionisio, A., Anselmi, S., Cesare, L., Massotti, P., Silvestrin. “The Next Generation Gravity Mission: challenges and consolidation of the system and AOCS concepts”. GNC Conference 2017, Salzburg, Austria.